Int. J. Nanosci. Nanotechnol., Vol. 9, No. 1, March 2013, pp. 33-38

Effect of Grinding Time on Structural and Thermal Properties of Strontium-Doped Nanostructural Lanthanum Manganite as SOFC Cathode Material

H. Tamaddon*, A. Maghsoudipour

Ceramics Department, Materials and Energy Research Center, Tehran, I. R. Iran

(*) Corresponding author: tmdn.imn.86@gmail.com
(Received:25 Nov. 2012 and Accepted: 03 Feb. 2013)

Abstract:
In this work, the strontium-doped lanthanum manganite- a ceramic material- used as cathode in solid oxide fuel cells. An impression of grinding time on the structural and thermal properties of Sr-doped $LaMnO_3$ system with $La_{1-x}Sr_xMnO_3$ (x=0.2) stoichiometric ratio was investigated. The nano crystallite LSM powder with cubic structure was prepared by varying the milling time of planetary monomill during the mechanochemical method. XRD diffraction patterns confirmed that increasing milling time has effect on phase structure, sintering and thermal behavior of LSM. The optimum sintering temperature was determined and then thermal treatments were investigated with Differential Thermal Analysis (DTA) and Thermal Gravimetric Analysis (TGA) methods, respectively. The results of this research certainly indicated that by increasing grinding time as an important factor in LSM mechanochemical synthesis, the nanocrystallite size and distribution as well as thermal characteristics will be modified.
Keywords: *Solid oxide fuel cell, Strontium-doped lanthanum manganite, Mechanochemicl synthesis, Cathode material, Nanocrystallite, Phase structure.*

1. INTRODUCTION

Solid Oxide Fuel Cells (SOFCs) are promising efficient, energy-saving, and environment-friendly energy conversion devices that generate electricity and heat. As one of the key materials of SOFC, strontium-doped $LaMnO_3$, especially 20 mol% Sr doped $LaMnO_3$ ($La_{0.8}Sr_{0.2}MnO_3$), is currently the preferred cathode material because of its high electronic conductivity [1], good compatibility with the solid electrolyte, 8 mol% yttria-stabilized zirconia (YSZ), in the oxidizing atmosphere [2]. Moreover, similar coefficient of thermal expansion to that of YSZ for practical use, and good chemical and thermal stability are the other beneficial properties of LSM [3].

The electrical conductivity and catalytic activity of lanthanum manganite are considerably enhanced when lanthanum is partially substituted with strontium [4]. Lanthanum strontium manganite is p-type electrically conducting oxide by ABO_3-type perovskite structure [5].

The improvement of electrochemical performances has been attributed to decreasing grain sizes, which allows spreading and growing of active sites at the electrolyte/electrode interface. This design modification is suitable for SOFC intermediate operating temperature. Thus, a low sintering temperature should be intended to take advantage of desirable features, such as small grain diameters [6].

Commonly, after LSM was produced it is

characterized primarily by its chemical (purity, homogeneity) and physical (particle size, surface area) properties. The ideal characteristics of an LSM powder for fuel cells, are the purity, with a perovskite structure, small average particle size and large surface area [7].
This paper shows that whilst these are still relevant criteria, the thermal and electrical properties of the powder must also be considered.

2. EXPERIMENTAL

MnO_2, La_2O_3, and SrO (Merck, with purity >99%) were used as starting reagents. MnO_2 was heated at 600°C for 12 hours in order to convert it into Mn_2O_3. The formation of single-phase Mn_2O_3 was confirmed by X-ray powder diffraction before its use. Later, the proper weight ratio of reactants: La_2O_3, Mn_2O_3, MnO_2, and SrO were completely mixed in acetone liquid media with an appropriate stoichiometric ratio as per reaction 1 [8].

$$0.4(La_2O_3+Mn_2O_3)+0.2(SrO+MnO_2) = La_{0.8}Sr_{0.2}MnO_3 \quad (1)$$

In order to investigate of the milling time effect on LSM phase formation a planetary monomill (PMV2-Tajhizceram Co.) was used for the ball milling. The batch of 50 g of the aforementioned mixture was taken into the zirconia bowl. Later, 15-mm diameter zirconia balls were added into it as ball/powder ratio was 15. The rotational speed of the planetary monomill was 300 rpm (revolution per minute).
Finally, after sampling in different grinding times the ground samples were calcinated at 600°C for 2 hours in air to complete the phase formation process as well as the removal of the possibly absorbed moisture and impurities. In order to compare the influence of milling process on LSM ceramic powder properties, one of the samples was not subjected to the milling operation and was kept as the evident sample. Species were coded based on table 1.
All the samples were characterized by X-ray powder diffraction method by X-ray diffractometer (Philips. Pw 3710 mpd control), with curved graphite crystal monochromator, and using Cu-Kα radiations in the 2θ range from 10° to 80°. In order to study of the phase formation and identification, the obtained X-ray powder diffraction (XRD) data were subjected to profile fitting, before analyzing with the help of X'pert Highscore plus software.

Table 1: *samples coding based on preparative parameters*

Sample code	Milling rpm	Milling time(hour)
S-0h-600c	-	0
S-3h-600c	300	3
S-12h-600c	300	12
S-24h-600c	300	24
S-36h-600c	300	36
S-48h-600c	300	48

For more physical and morphological study of mechanically prepared powder particle size, distribution and specific surface area the BET test was carried out with Gemini 2375 model instrument (Micromeritices company). Prior to BET analysis, the samples were outgassed for 24h at 150°C. Microstructure of cathode powders was investigated by scanning electron microscopy using a S360 Cambridge 1990 tool. Prior to this test the samples were coated with a thin layer of gold and the acceleration voltage was 20 kV, using secondary electron scattering.
The differential thermal analysis–thermogravimetry (DTA–TG) of the powder sample was carried out at a heating rate of $5^oC.min^{-1}$ by a DTA–TG unit (model PL-STA 1640, England) in air. The thermal expansion was monitored by means of a dilatometer tool (model DIL 402E Netzsch, Germany) at a rate of $10^oC.min^{-1}$. Dimensions of the prepared samples were 50×5×5 mm for length, width and height, respectively.

3. RESULTS AND DISCUSSION

3.1. Phase formation

The diffraction patterns of not-milled and milled powder samples which calcinated at 600°C are illustrated in Figure 1. As can be seen, diffracted lines of not ground powder-sample well accord with primary oxide ingredients as well as a compound of

principle elements without any dopant ($LaMn_2O_5$). For the samples which milled for 12h and more, compared with ideal perovskite $LaMnO_3$ pattern (JCPDS:75-440) the diffraction peaks indexed well to perovskite structure with cubic symmetry as this phase formation process was completed along with grinding time increase. This suggested that Sr^{2+} was successfully incorporated into the A-site (Lanthanume situation) of the LSM lattice. Moreover, the presence of sharp main peak at around 32° degree and also decrease of noise amount during with milling time increase, confirm the single phase LSM formation.

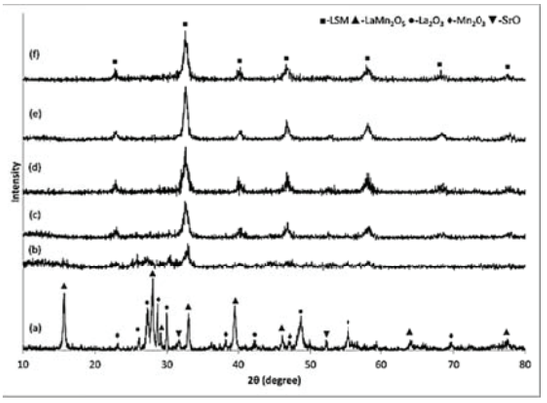

Figure 1: *X-ray powder diffraction patterns of S-0h(a) not milled and S-3h-600c(b), S-12h-600c(c), S-24h-600c(d), S-36h-600c(e) and S-48h-600c(f) ground samples with 300 rpm which obviously expose sharp peaks corresponded to cubic structure*

3.2. Crystallite size and specific surface area

The average particle size (D^*_{BET}) was calculated assuming the presence of spherical particles, by means of the equation 2 [9]:

$$D^*_{BET} = 6/(\rho.S_{BET}) \quad (2)$$

Where ρ is the theoretical density of LSM (6.6 $g.cm^{-3}$) and S_{BET} is the specific surface area.

As can be seen in Figure 2, the measured surface area has an optimum amount, where the BET amount has a maximum point. By grinding duration increase, the granulation phenomenon cause to surface area decrease. As the XRD broadened pattern confirm, in optimum case that related to 24-hour milled sample, the particle diameter decrease to about 50 nm which is the lowest particle size among the ground nanopowder samples.

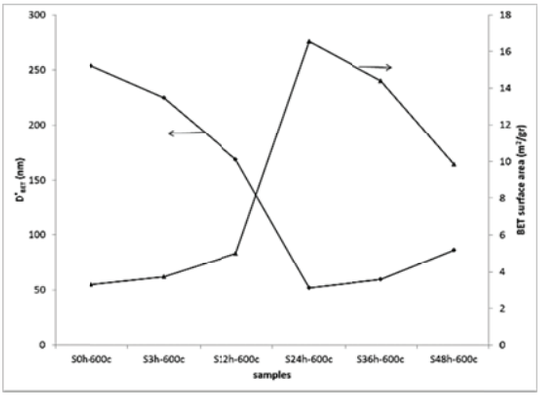

Figure 2: *BET surface area (m^2/gr) contrast to D^*_{BET} (nm) for LSM ground samples*

3.3. Thermal analysis

3.3.1. Thermal decomposition

Typical thermograph of the raw precursor and 48h-milled powder samples are depicted in Figures 3,4, respectively. In Figure 3 that is related to not milled LSM powder sample, there is a 6-step weight loosing trend during temperature increasing. As can be seen in Figure 4 which is related to the DTA and TG graphs of 48h-milled sample, there is a gradually single-step weight decreasing mode.

Generally, in comparison the as received LSM powder sample suffers from a drastic weight loss around 12%, whereas 48h-ground sample exhibits only 4% weight loss. According to the TG curve in Figure 3, there is a weight increase around 0.4% between 40-60°C which is possibly because of water crystallization [10], while the next 0.6% weight increase stage from 90-280°C could be related to the composition of $Sr(OH)_6$ from primary SrO precursor [11].

The observed weight loss of 5.2% within 280-340°C may be due to the decomposition of La_2O_3[12] which is confirmed by an endothermic peak in DTA plot. The next step of weight loss which is 3.1% at the temperature range of 420-480°C as well as 0.8% weight loss between 620-680°C are infered to a decrease in Mn ionic valency from Mn^{+4} to Mn^{3+} and phase transformation of MnO_2 from α

to γ respectively [11,12]. This phase transition is affirmed by endothermic peak of DTA curve. The last weight loss of 0.5% along 720-840°C can be pertained to complete decomposition of carbonates and initiation of LSM phase formation [13]. At the temperature range more than 900°C there is a slight weight increase of 0.4% which is corresponded to LSM formation of unreacted substances in the not milled powder mixture [14].

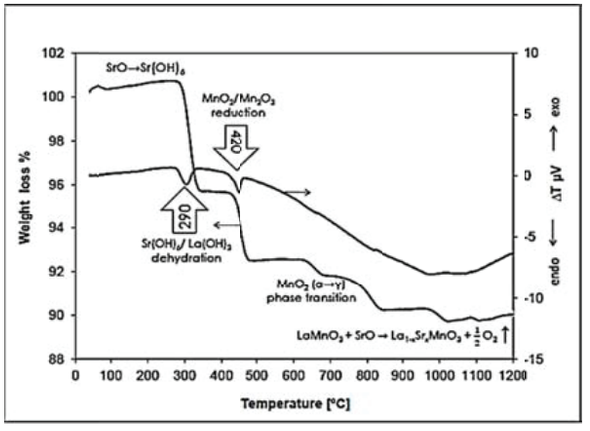

Figure 3: *TGA and DTA curves of the not milled sample before subjecting to calcination*

According to the DTA and TG plots which are illustrated in Figure 4 the weight loss trend for 48h-milled sample includes just one step which gradually occurs within 60-1200°C along with weight loss of around 4.5%. This could suggest that principle decomposition and single-phase formation reactions are perfectly completed during the grinding operation as there is no peak in the DTA plot of this sample.

3.3.2. Thermal expansion

Figure 5 depicts the comparative dilatometric curves and variation mode of thermal expansion coefficient (TEC) for S-0h-600c and S-48h-600c samples. It exhibits an increase in the thermal expansion ($\Delta L/L_0$) with increasing temperature. As can be seen, up to around 400°C, the expansion behavior of both samples are similar, however, within temperature increase the not milled sample have a little difference with 48h-milled sample.

It can be explained that grinding process cause an structural improvement in LSM lattice. As a matter of fact the general thermal behavior of ideally substituted Sr in it is alike $LaMnO_3$ host oxide. The change trend of TEC (α) which is inserted in Figure 5 indicates that before almost 700°C, the not milled LSM have more TEC amount while after this point the ground LSM sample comprises further thermal expansion coefficient. It elucidates that the thermal procedure have an optimum temperature.

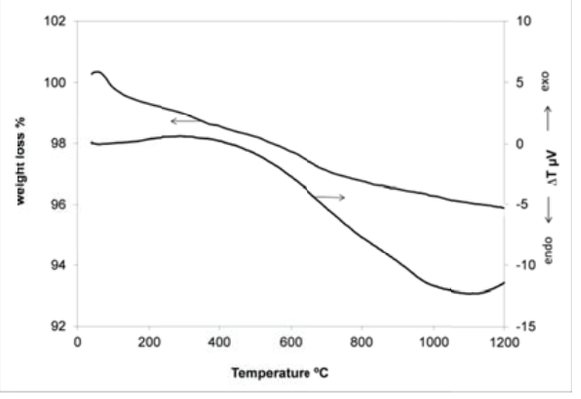

Figure 4: *TGA and DTA thermograms of the 48h-ground powder sample prior to be calcinated*

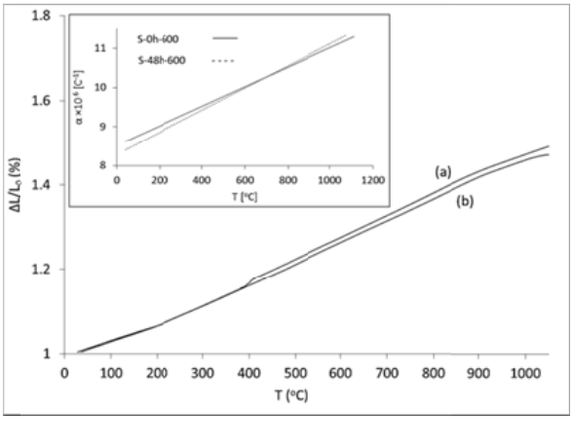

Figure 5: *Thermal expansion ($\Delta L/L_0$) curves of the S-0h-600c (a) and S-48h-600c (b) samples for the temperature range of 38-1200°C and insert exhibits variation of the coefficient of thermal expansion (α) for the temperature region of 38–1112°C*

3.4. Morphology

The morphology of calcinated powders obtained

at different milling times can be seen in Figure 6. A close examine of Figure 6 reveals the milled samples reached fine particles with homogeneous distribution. Moreover, formation of small aggregates for all samples are obvious.

The amount and size of these aggregates corresponded to BET test results increase for the powder samples which milled more than 24 hours. This was pointed out XRD patterns confirmed the formation of fine and well-distributed perovskite particles after 12h of high energy grinding as can be seen here. Also based on the XRD and BET examination results the nanocrystalline LSM samples formed during the mechanochemical process are surface-activated, and the degree of activation depends on the surface/ bulk atom ratio [8,15].

In principle, activation of the surface naturally relaxed by the agglomeration of crystallites concurrently. So the milled nanopowder samples with grinding time period longer than the optimum amount consist of grains with smaller crystallite size. As a result they have more degree of agglomeration.

4. CONCLUSION

In order to obtain the perovskite LSM phase with cubic symmetry by mechanochemichal method with rotational speed of 300 rpm, the optimum milling time is 36-hour. This outcome was confirmed by relevant high specific surface area and morphological study with SEM images. It is worth mentioning here that the grinding operation strongly affects on thermal decomposition of LSM. However the influence of this process on the thermal expansion of LSM was not very sensible. This concluded that, milling procedure could be sensibly improve the structural and thermal properties of LSM without further chemical consideration.

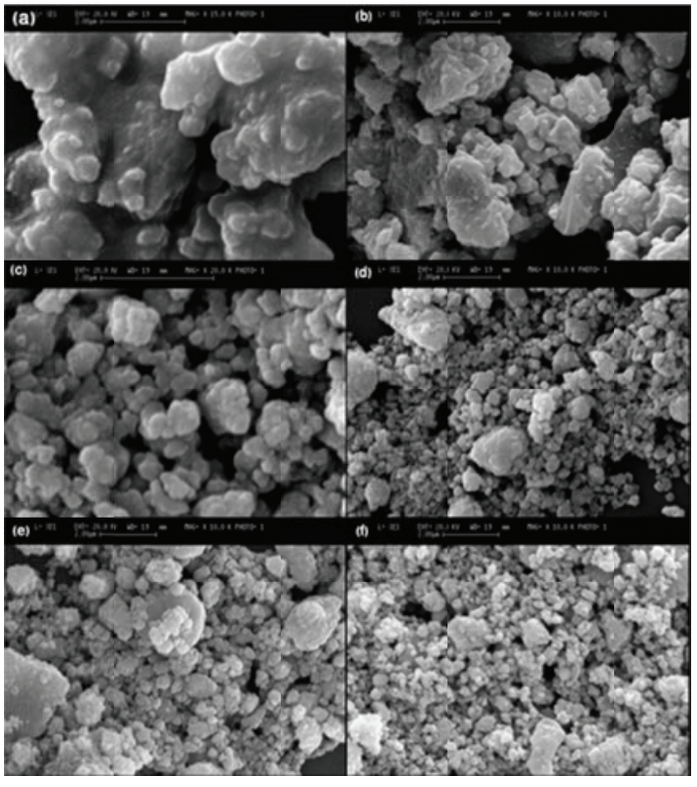

Figure 6: *SEM images of S-0h(a), S-3h-600c(b), S-12h-600c(c), S-24h-600c(d), S-36h-600c(e), S-48h-600c(f). The cathode materials were calsined for 2 h at 600*

ACKNOWLEDGMENTS

This technical effort was performed in support of Materials and Energy Research Center. The authors also would like to gratefully acknowledge to professor M. Kianpour for his worthwhile consults.

REFRENCES

1. L.G. De Haart, R.A. Kuipers, K.J. De Vries: J. Electrochem. Soc., Vol. 138, (1991), pp. 1970–1975.
2. H. Taimatsu, K. Wada, H. Kaneko: J. Am. Ceram. Soc., Vol. 75, (1992), pp. 401–405.
3. S. Otoshi, H. Sasaki, H. Ohnishi: J. Electrochem. Soc., Vol. 138, (1991), pp. 1519–1523.
4. S.P. Jiang: J. Mater. Sci., Vol. 43, (2008), pp. 6799–6833.
5. F. Zheng, L. R. Pederson: Electrochem. Soc., Vol. 146, (1999), pp. 2810-2816.
6. R.M. Belardi, J. Deseure, M. Caldeira, B. Matencio, R.Z Domingues: Ionics, Vol. 15, (2009), pp. 227–232.
7. R.J. Bell, Graeme J. Millar, J. Drennan, Solid State Ionics, Vol. 131, (2000), pp. 211–220.
8. K.R. Nagde, S.S. Bhoga: Ionics, Vol. 16, (2010), pp. 361-370.
9. L. Conceicao, C.R.B. Silva, N.F.P. Ribeiro, M.V.M. Souza: Mater. Charact., Vol. 60, (2009), pp. 1417–1423.
10. K.R. Nagde, S.S. Bhoga: Ionics, Vol. 15, (2009), pp. 571–578.
11. R.C. Mackenzie, Differential Thermal Analysis, Academic press. London and NewYork, Vol. 1, Ch. 9, (1970), pp. 286-290.
12. A. Ianculescu, A. Braileanu, M. Zaharescu, I. Pasuk, E. Chirtop, C. Popescu and E. Segal: J. Therm. Anal. Calorim., Vol. 64, (2001), pp. 1001-1010.
13. A. Ghosh, A.K. Sahu, A.K. Gulnar, A.K. Suri: Scr. Mater., Vol. 52, (2005), pp. 1305–1309.
14. J. Chaichanawong, K. Sato, H. Abe, K. Murata, T. Fukui, T. Charinpanitkul, W. Tanthapanichakoon and M. Naito: Adv. Powder Technol., Vol. 17, (2006), pp. 613–622.
15. A. Lanzini, P. Leone, P. Asinari: J. Power Sources, Vol. 194, (2009), pp. 408–422.